Numerical and experimental validation and comparison of reduced order models for small scale rotor hovering performance prediction

Numerical and experimental validation and comparison of reduced order models for small scale rotor hovering performance prediction

M. Carreño Ruiz *, A. Manavella † and D. D'Ambrosio ‡
Department of Mechanical and Aerospace Engineering, Politecnico di Torino, Torino, 10124, Italy

Unmanned Aircraft Systems (UAS) are state of the art in the aerospace industry and are involved in many operations. While initially developed for military purposes, commercial applications with small-scale UAS, such as multicopters, are today frequent. Accurate engineering tools are required to assess the performance of these vehicles and optimize power consumption. Thrust and power curves of rotors used by small-scale UAS are essential to design efficient systems. The lack of experimental data and accurate prediction models to evaluate rotor coefficients over the UAS flight envelope are two substantial limitations in UAS science. In addition, Reynolds numbers based on the chord for small-scale rotors at usual rotation rates are usually smaller than $100,000$ resulting in degraded performance. In this paper, we describe two in-house Reduced Order Models (ROM's), namely a Blade Element Momentum (BEM) code and a Non-Linear Lifting Line Theory approach combined with Free Vortex Wake (NLLT-FVW) code. We verify these models with three-dimensional Computational Fluid Dynamics (CFD) simulations, and we validate them with existing experimental data for blades in low Reynolds conditions. We also use two-dimensional CFD simulations to generate the aerodynamic database for the reduced-order models.

I. Nomenclature

$C_Q = \frac{Q}{\rho\pi\Omega^2R^5}$	=	rotor torque coefficient
$C_T = \frac{T}{\rho\pi\Omega^2R^4}$	=	rotor thrust coefficient
$C_P = \frac{P}{\rho\pi\Omega^3R^5}$	=	rotor power coefficient
FM	=	rotor figure of merit
$C_l = \frac{l}{\frac{1}{2}\rho V^2 c}$	=	airfoil lift coefficient
$C_d = \frac{d}{\frac{1}{2}\rho V^2 c}$	=	airfoil drag coefficient
c	=	airfoil chord
V	=	freestream velocity
l	=	airfoil lift
d	=	airfoil drag
D	=	rotor diameter
Ω	=	rotation rate in radians per second
RPM	=	rotation rate in revolutions per minute
R	=	rotor radius
Re	=	rotor Reynolds number computed at 75% propeller radius
Re_c	=	rotor Reynolds number based on the chord
M	=	rotor tip Mach number
T	=	rotor thrust

*PhD Student, Department of Mechanical and Aerospace Engineering, Politecnico di Torino, C.so Duca degli Abruzzi, 24, 10124 Torino, Italy, manuel.carreno@polito.it

†MSc Student, Department of Mechanical and Aerospace Engineering, Politecnico di Torino, C.so Duca degli Abruzzi, 24, 10124 Torino, Italy, s263200@studenti.polito.it

‡Adjunct Professor, Department of Mechanical and Aerospace Engineering, Politecnico di Torino, C.so Duca degli Abruzzi, 24, 10124 Torino, Italy, domenic.dambrosio@polito.it

Q	=	rotor torque
P	=	rotor power
ρ	=	air density
γ	=	intermittency
k	=	turbulent kinetic energy
Re_θ	=	momentum thickness Reynolds number
ω	=	specific dissipation rate

II. Introduction

The high cost of Computational Fluid Dynamics (CFD) evaluations of rotor blades makes the availability of Reduced Order Models (ROMs) mandatory in the early design phases. The Blade Element Momentum (BEM) method is a fast and reasonably accurate tool when the blades work at high Reynolds numbers and have high aspect ratios. When the Reynolds number drops and two-dimensional flow is no longer guaranteed, the accuracy of this approach is compromised, especially in hovering conditions. On the other hand, the NLLT-FVW method is much more demanding than the BEM method, but it takes into account the modeling of the wake and therefore performs a more accurate estimation of the inflow angles, as shown for example in [1]. The cost of the Free Vortex Wake approach is generally three orders of magnitude more expensive than BEM, and even four orders of magnitude in some slow convergence cases, such as in hovering simulations. In any case, its cost is always between 4 and 5 orders of magnitude cheaper than CFD calculations. In this paper, we compare the accuracy and the computational cost of simulations of hovering rotor performance using different fidelity approaches.

We used the BEM code described in [2], which we modified with the addition of the viscous swirl correction presented in [3]. The NLLT-FVW is described in [4] and it follows the theory presented in [5]. This code was verified with the open-source code Qblade [6], which is also based on the theory in [5]. The blade used in this study is the T-motor 15"x5" Carbon Fiber, which was tested previously experimentally (see [7, 8] among others). The CFD simulations follow the work presented in [7], where a numerical validation of the experimental data in [2] was performed with a satisfactory agreement.

To build an aerodynamic database for the T-motor blade, we followed a critical station approach for selecting appropriate radial stations to compute the polar curves. Such stations must allow a reasonable interpolation of geometrical airfoil characteristics to obtain accurate values of lift and drag, which, in a first analysis, could be associated with camber and thickness. To this purpose, we chose five different typical airfoil sections, and we computed their polar curves for a reasonable range of angles of attack and Reynolds numbers. Considering that the Reynolds number over the blade falls in the very-low regime ($2 \cdot 10^4 - 2 \cdot 10^5$) where we expect a separation-induced transition, we carried out the simulations coupling the γ-Re$_\theta$ transition model [9] to the $k-\omega$ turbulence model[10].

III. Geometry

We obtained the T-motor 15x5 CF blade geometry using an optical precision measuring machine (OPMM) that allowed us to perform accurate two and three-dimensional simulations. The scanning of the blade generated a cloud of points defining the outer surface of the blade. We sliced the cloud of points with planes normal to the radial direction with a separation of 5 mm to capture accurately strong gradients in this direction which are especially important in the inner part of the blade. We interpolated the intersection points with a smooth spline, and we generated a guide curve using the points defining the leading and trailing edges. A lofting process allows the generation of a smooth manifold surface, which is appropriate for CFD simulations. Figure 1 shows the top and front views of the reconstructed geometries compared with images of the original rotor. Furthermore, the ROMs require information about the blade geometry at every radial station, such as the chord, twist, and quarter-chord position distributions. We obtained these data from the reconstructed CAD model which was sliced to compute local airfoil properties.

IV. Aerodynamic database

A reasonably accurate interpolation requires that the radial discretization be fine enough to capture variations in camber and thickness distributions. Here we propose to discretize the blade geometry using five sections located at a relative radial position of 0.28, 0.53, 0.78, 0.91 and 0.99. Table 1 shows the interpolation strategies between stations.

Figure 3 shows clear non-linearities in the aerodynamic efficiency of the airfoils which are due to reattachment of the

Fig. 1 Top and front views comparison between original blade(Left) and reconstructed CAD model(Right).

Table 1 Interpolation strategy between stations.

r/R	Initial Polar	Final Polar	Interpolation
0.15<r/R<0.28	28%	28%	Constant
0.28<r/R<0.53	28%	53%	Linear
0.53<r/R<0.78	53%	78%	Linear
0.78<r/R<0.91	78%	91%	Linear
0.91<r/R<99	91%	99%	Linear
0.99<r/R<1	99%	99%	Constant

flow forming a separation bubble. It is also clear how the value of the efficiency drops one order of magnitude between the highest and lower Reynolds numbers. Figure 2 shows how as the radial coordinate increases, the curvature of the airfoils decreases and thickness initially decreases and then grows again near the tip section. This trend is coherent with the value of aerodynamic efficiency which drops by a factor of three comparing the highest and smallest cambered sections. Figure 4 shows an example of a separation bubble forming on the suction side of the airfoil. The ability to reproduce this separation bubbles is important as its presence generates a transitional ramp, as described by [11], in the polar of the airfoils which causes lift and drag coefficients to scale linearly instead of the usual parabolic scaling observed at higher Reynolds numbers. This aspect shows how including a transition model able to capture separation bubbles is crucial as shown in [12]. Most aerodynamic databases present in literature to be used in reduced order models, such as the blade element method, use Xfoil[13] or similar panel method codes to compute their polars as they obtain impressive accuracy considering their computational cost as shown by [14, 15] which compare xfoil calculations with implicit large eddy simulations. While the flow is attached and steady, CFD calculations and Xfoil calculations will be close as both include a transition model and the integral boundary layer method embedded in Xfoil has proven to to be accurate in these cases. However, if the flow separates, Xfoil and CFD calculations might differ considerably and this scenario is typical of very low and ultra low Reynolds numbers as shown in [16]. For Reynolds numbers below 15,000 the laminar solver was used, above this value the $k-\omega$ turbulence model[10] was used in combination with the γ-Re_θ transition model[9]. The reason for the use of laminar simulations for the lower Reynolds numbers is that for ultra low Reynolds numbers a laminar separated unsteady regime is generated which causes a high lift due to the reduced pressure associated to the high velocities caused by the vortex emission[1]. This regime is shown to be damped by the transition model and do not always capture this regime especially for larger angles of attack where this highly empirical model predicts a premature transition for Reynolds numbers as low as 3000.

V. BEM simulations

This implementation follows the classical double link approach and iterates until momentum theory and blade element theory induction factors converge. The BEM code is an adaptation of the one presented in [2] including the classical angular momentum correction to account for the viscous swirl detailed in [3] and the widely used Prandtl's tip and hub loss corrections shown in [17] among others. The influence of the viscous swirl correction for typical MAV's

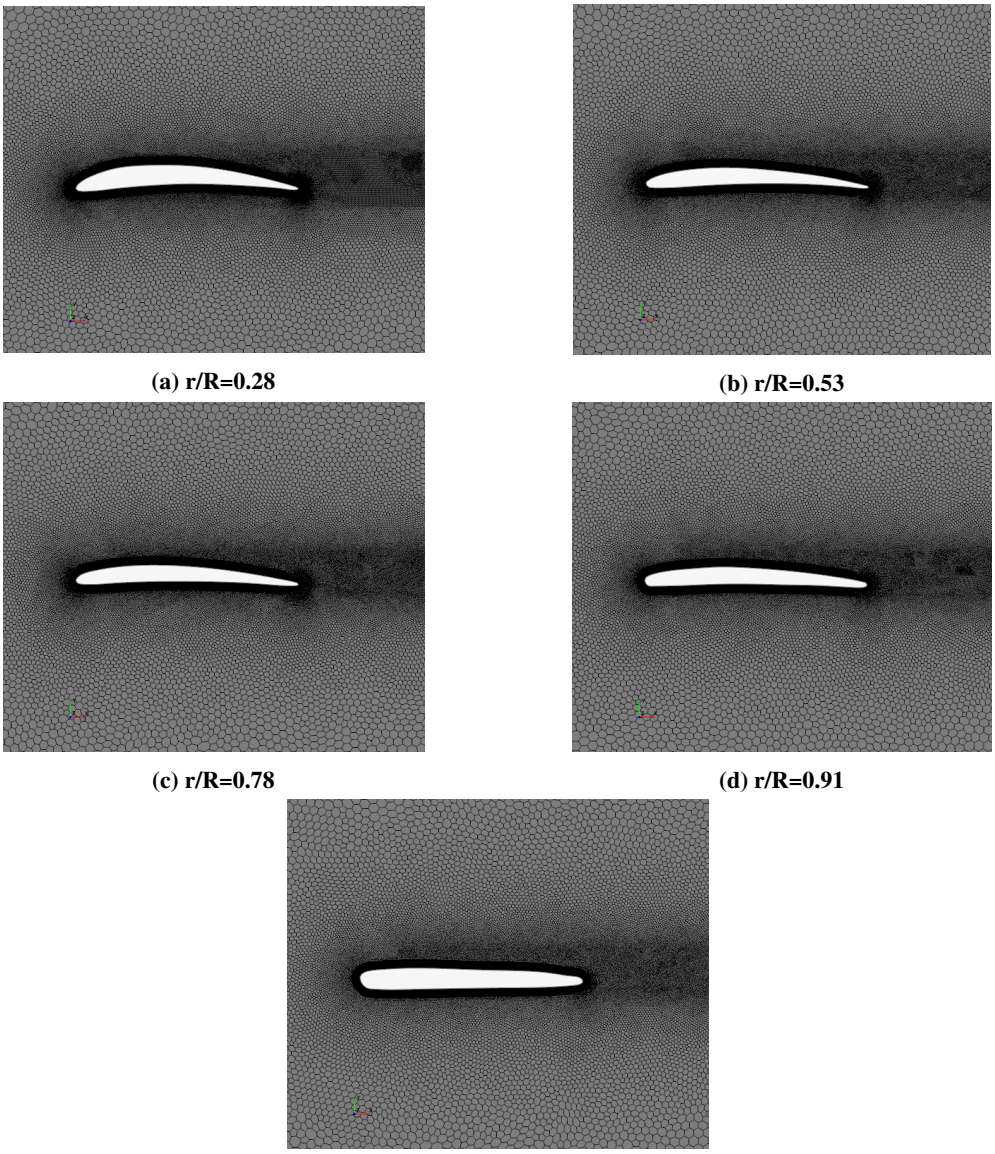

(a) r/R=0.28 **(b) r/R=0.53**

(c) r/R=0.78 **(d) r/R=0.91**

(e) r/R=0.99

Fig. 2 Airfoil sections for which the polar is calculated including computational mesh for an angle of attack of 0º.

Reynolds numbers should be small, but we maintained it for completeness as this correction is asymptotic and tends to 0 with the inverse of the aerodynamic efficiency.

The BEM code requires geometrical input defining the blade. These inputs consist of the chord and twist radial distributions. The BEM performance is the fastest within the rotor design tools with a computational cost around 10^{-4} CPU hours. The speed and simplicity of this code makes it one of the most used for design applications. For large Reynolds numbers and large aspect ratios of the blades the hypothesis for which the theory was derived are satisfied, however for very low Reynolds numbers, aerodynamically efficient blades have smaller aspect ratios [1, 18]. This compromises the accuracy with which local angles of attack are predicted which are essential for design purposes. This fact is evidenced by [1, 19] for ultra low Reynolds number.

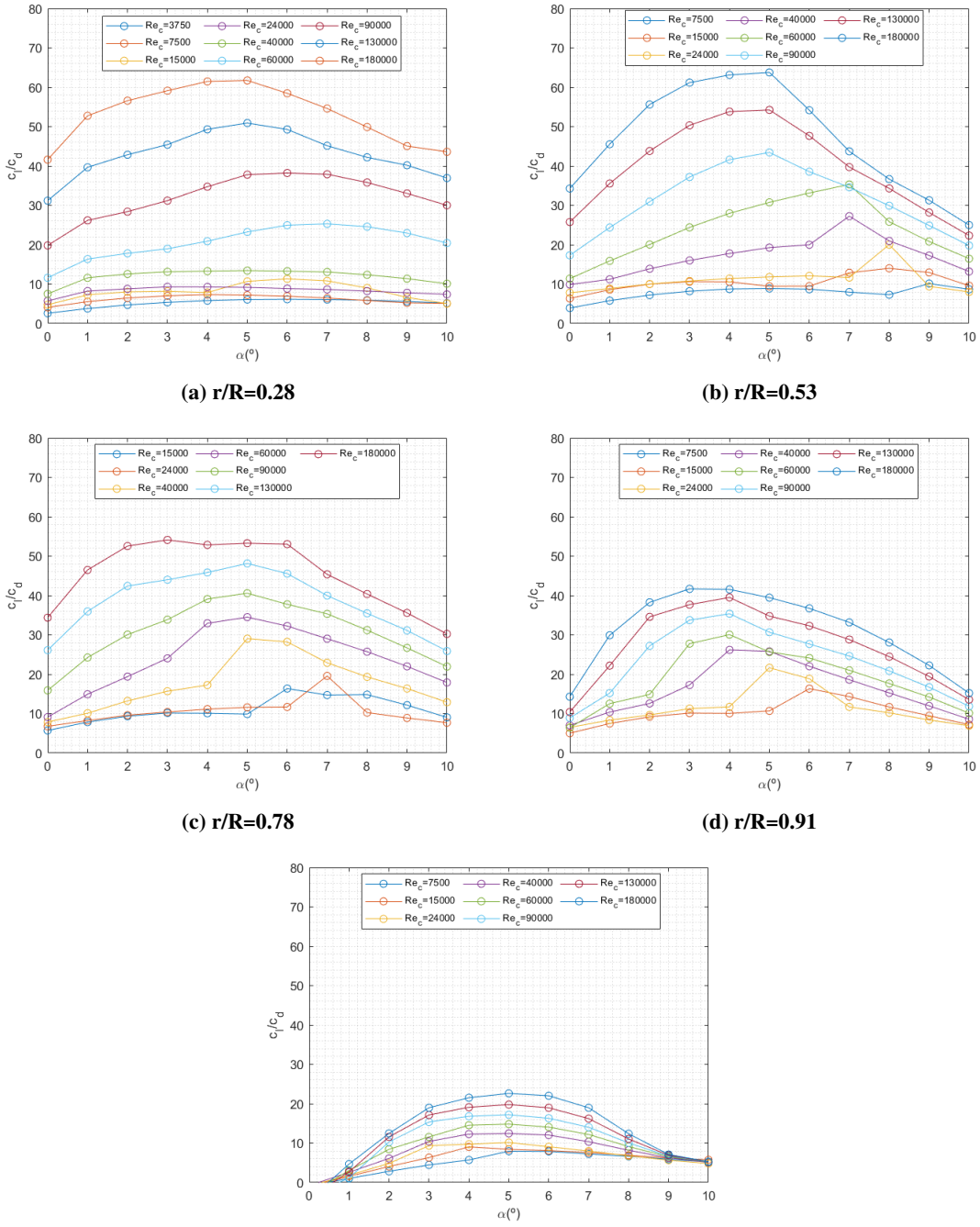

(a) r/R=0.28

(b) r/R=0.53

(c) r/R=0.78

(d) r/R=0.91

(e) r/R=0.99

Fig. 3 Aerodynamic efficiency at different radial stations, Reynolds number and angles of attack.

VI. NLLT-FVW simulations

This code is implemented in MATLAB and was originally developed by [4]. It employs the lifting line theory for the rotor model, which is made non-linear due to the inclusion of the polar of the airfoil, which is vital at these low Reynolds numbers where the lift curves become non-linear. We combine the rotor model with a Free Vortex Wake (FVW) method to model the wake, which is left free to deform based on the velocities induced by the whole vortex system generated by the rotor. At each time step, we implemented an iterative approach until the circulation on the blade reaches an

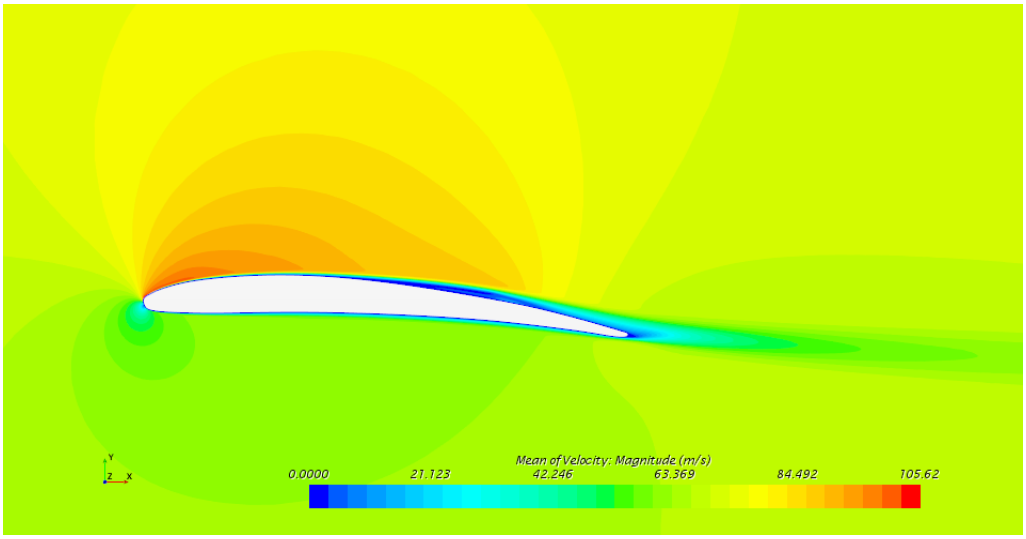

Fig. 4 Velocity magnitude of the flow around the airfoil at 53% of the radial coordinate at a Reynolds number of 90,000 at an angle of attack of 4º.

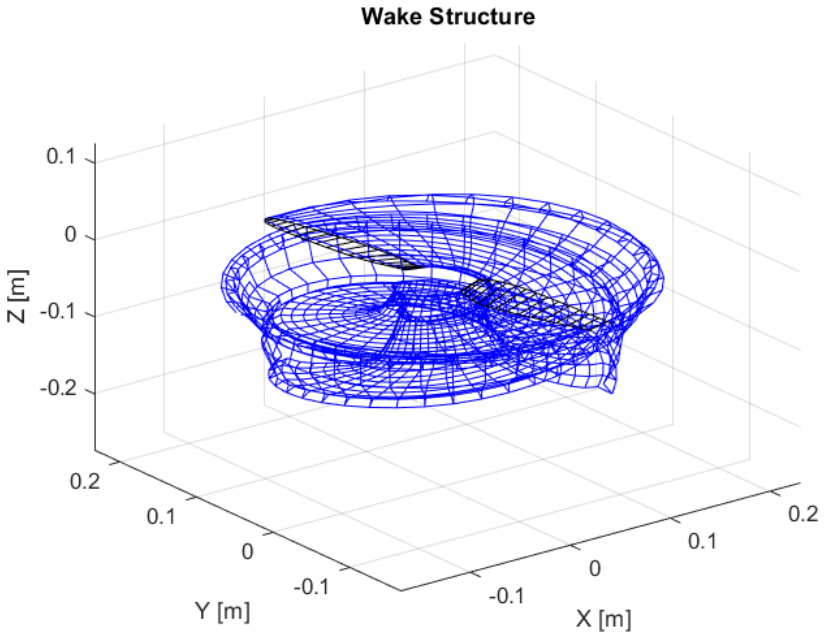

Fig. 5 Vortex filaments forming the wake behind a hovering Tmotor 15x5 after 1 revolution.

asymptotic behavior. We calculate the induced velocities using a desingularized version of the Biot-Savart law. The desingularization follows Van-Garrel's approach [5], but we added a modification to maintain dimensional consistency. The aim of this correction is to reduce the influence of the rotor scale with the model parameters. Reference [4] shows that such a correction produces a better approximation of the blade loading but tends to compromise the solver stability, especially in hovering calculations where the vortex system is auto-induced and lacks an inflow which tends to stabilize this vortex system[20]. A Lamb-Oseen viscous core model, as shown in [21] is included to allow the vortex to grow in time due to dissipation effects, and a correction is applied to the viscous core radius to account for the vortex stretching effect [22]. This model possesses two parameters that represent a compromise between robust induction and solution stability. References [4, 22] contain a thorough analysis of the effects of these parameters. The induction of all the

vortex filaments on all the vortex nodes must be computed at every time step. Since the number of vortices grows linearly with time, the computational time has a quadratic relationship with the number of revolutions. This fact makes the computational cost sensible to the solver setup and inflow conditions. In any case, the computational cost is between 10^{-1} and 1 CPU hours, significantly smaller than CFD simulations. The induction step is fully parallelized which allows significant reduction of the simulation time when multiple processors are available.

Figure 5 shows 1 revolution of the vortex wake structure obtained for the test case shown in section VIII corresponding to the lowest Reynolds number. It is clear how the wake rolls round the tip vortex and how the passage of this is very close to the blade due to the hovering condition. The rotor is sliced with a cosine spacing to concentrate more filaments near root and tip to capture accurately these vortices. The simulation time corresponds to 10 rotor revolutions which has proven sufficient for the thrust and torque values to converge both locally and globally.

VII. CFD simulations and experimental validation

We used the commercial CFD code STAR-CCM+ for these simulations. We performed the experimental validation simulating the experimental setup as shown in Figure 6. We chose the operation conditions of the propeller to match available experimental data from a campaign described in [2] in a climatic chamber (TerraXcube) where it is possible to control pressure and temperature to simulate high altitudes and hence the Reynolds number can be modified. Three conditions comprising very different Reynolds numbers are analysed in this paper as shown in table 2. We used a time-accurate sliding mesh Unsteady Reynolds Averaged Navier-Stokes (URANS) approach, with a time step equivalent to an angular displacement of 0.5º. The γ-Re$_\theta$ transition model [9] was included as the two dimensional polar indicates the presence of laminar-induced transition for the highest Reynolds number. The computational cost of a CFD simulation with the appropriate temporal and spatial discretization is over 2000 CPU hours using Intel Xeon Scalable Processors Gold 6130 2.10 GHz.

The experimental data shown in figure 7 reveals a linear relationship between C_T and Reynolds number, with degraded thrust coefficient values as lower Reynolds numbers are considered. An asymptotic behaviour is reached for the highest values of the Reynolds numbers. Thrust coefficient drops due to the effect of delayed transition and the eventual formation of separated flow regions that may reattach in the form of laminar separation bubbles. Previous studies such as [23] point out a critical Reynolds of 120,000 below which the effects of laminar separation become important and very sensitive to operating conditions that might affect transition. Above this limit rotor performance shows an asymptotic behaviour. This is in good agreement with our experimental results and particularly clear in figure 7c where the figure of merit shows an almost linear increase with increasing Reynolds numbers until approximately 120,000 where an asymptotic evolution is seen. Our CFD results using a transition model are in good agreement with the trends that show the non dimensional coefficients that characterize rotor performance. Regarding the comparison with experimental data provided by Russel [8], the asymptotic value of thrust and torque seems to be in good agreement. However there seems to be a slight overestimation of both thrust and torque values for lower Reynolds numbers. For further details on the CFD simulations and experimental validation please refer to [7].

(a) Experimental setup[2]

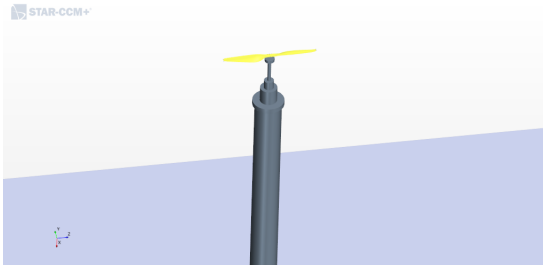

(b) Numerical setup

Fig. 6 Comparison between experimental and numerical setup

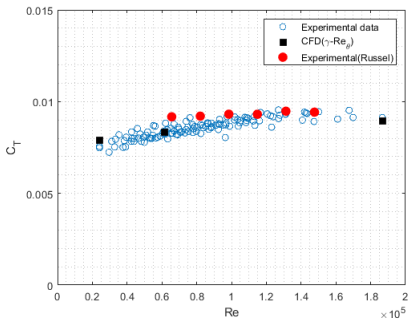

(a) Thrust coefficient for isolated rotor tests compared with CFD results and experimental data from [8]

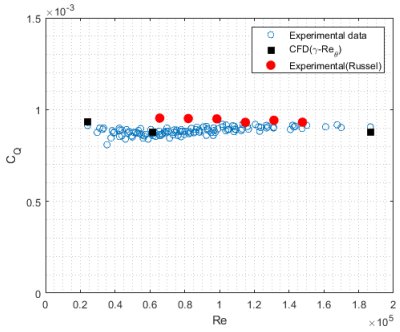

(b) Torque coefficient for isolated rotor tests compared with CFD results and experimental data from [8]

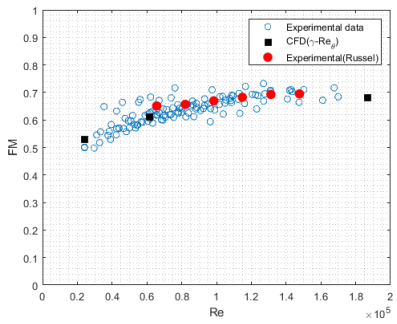

(c) Figure of merit for isolated rotor tests compared with CFD results and experimental data from [8]

Fig. 7 Experimental testing in terraXcube laboratory[2]

VIII. Performance comparison

Figure 8 shows a local comparison between the thrust and torque per unit length predicted by the ROMs and the CFD evaluations. Table 3 displays the integral values of thrust and torque including the experimental results performed by [2]. The thrust and torque integral values are in good agreement with experimental values, presenting errors below 10%. Regarding the comparisons along the radial coordinate, the BEM method presents an overestimation of the local thrust for intermediate blade positions, possibly associated with underestimated inflow angles. On the other hand, the vortex method shows a better local agreement, showing an overestimation of thrust and torque towards the tip region compared to CFD results. This is possibly due to the combination of considering a finite chord in the tip section and the inability for a lifting line rotor model to reproduce the complex three dimensional flow at the tip that only full CFD can attempt to model. We can also appreciate an inflexion point in the local thrust distribution at around 80% of the radial coordinate. This inflexion point is associated to the first passage of the tip vortex from the opposite blade below the original blade. This is the reason why only CFD and NLL-FVW, which model the evolution of the wake, are able to capture it. This characteristic is very important in hovering simulations where the passage of the first vortex is much closer to the blade compared to cases with a larger inflow velocity.

Reynolds number	Pressure(Pa)	Temperature(ºC)	RPM
24,099	30,900	40.05	3293
61,539	58,000	19.91	3979
186,670	98,450	-40.85	4683

Table 2 Test cases used to compare with numerical simulations.

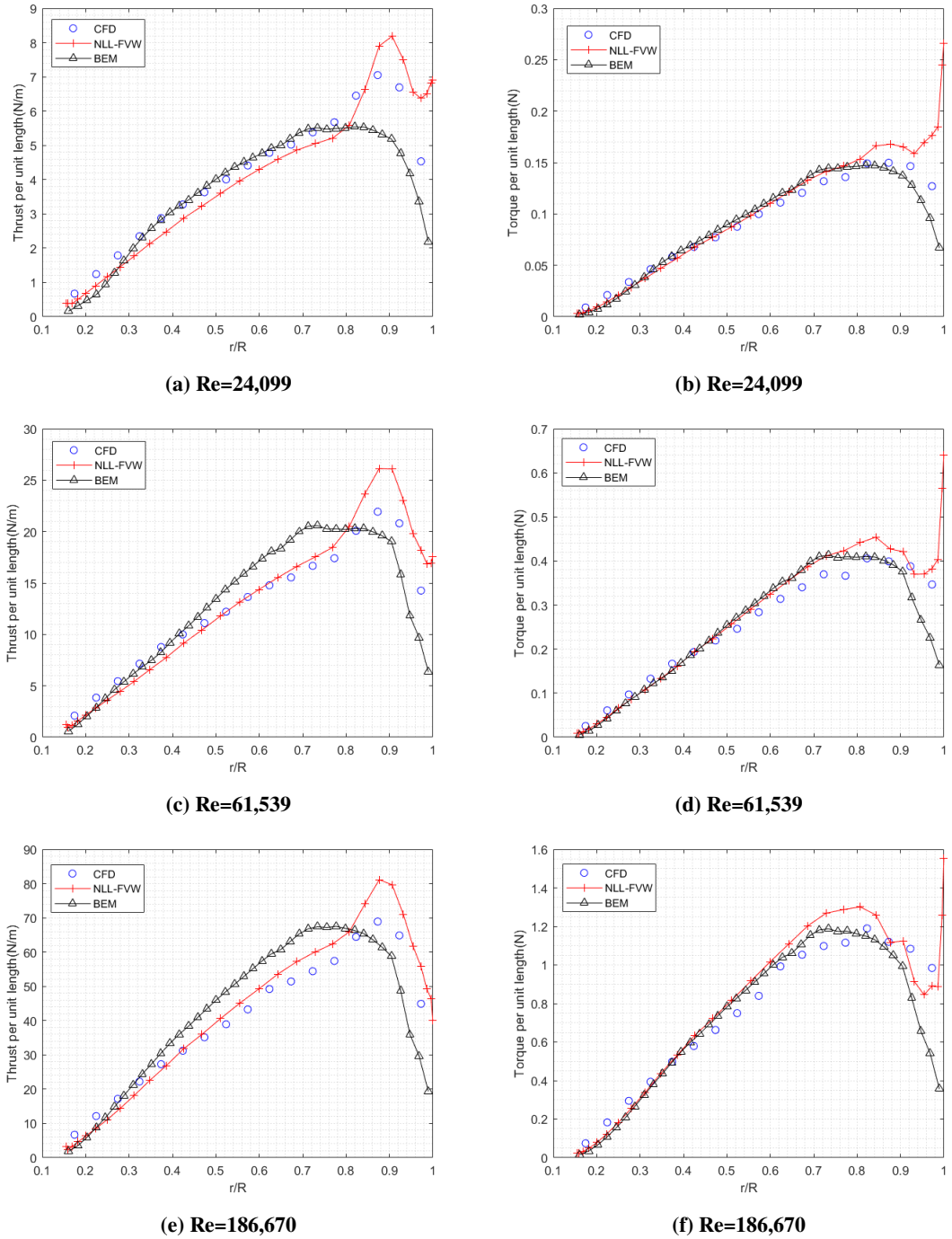

(a) Re=24,099 **(b) Re=24,099**

(c) Re=61,539 **(d) Re=61,539**

(e) Re=186,670 **(f) Re=186,670**

Fig. 8 Influence of different fidelity solvers on the thrust and torque radial distributions for different Reynolds numbers.

Table 3 also shows how the computational cost for performance calculation as we enhance the fidelity of the approach increases several order of magnitudes. On the other hand the increase in accuracy of the integral performance of the blade is quite limited.

	BEM		NLL-FVW		CFD		Experimental	
Re	**T [N]**	**Q [Nm]**	**T [N]**	**Q [Nm]**	**T [N]**	**Q [Nm]**	**T [N]**	**Q [Nm]**
24,099	1.19	0.029	1.29	0.032	1.33	0.030	1.26	0.029
61,539	4.18	0.082	4.24	0.088	4.12	0.083	4.16	0.082
186,670	13.80	0.236	13.88	0.257	13.16	0.0246	13.41	0.253
CPU time(h)	0.0003		0.5		2000		-	

Table 3 Different fidelity numerical solvers and experimental[2] rotor performance for different Reynolds numbers.

IX. Conclusions

We discussed and validated different methodologies for the calculation of rotor performance in hovering conditions. The computational costs vary a few orders of magnitude, whereas the fidelity of the approaches produces small percentages of improvement. Depending on the application, a few degrees might strongly impact performance, justifying the highest cost approaches. The NLLT-FVW technique seems a reasonable compromise choice between accuracy and computational cost as the inclusion of the wake modelling produces an enhanced agreement in local thrust distribution compared to the Blade Element Momentum Method. CFD is quite expensive for design applications. However, it is a powerful tool for validation activities, as shown in this paper, and its use becomes mandatory to explore exotic design conditions such as Martian, or terrestrial high-altitude aerodynamics, where three-dimensional effects might become significant due to the unique combination of low Reynolds numbers and high Mach numbers.

References

[1] Bézard, H., Desert, T., Moschetta, J.-M., and Jardin, T., "Aerodynamic design of a Martian micro air vehicle," *EUCASS 2019*, MADRID, Spain, 2019. URL `https://hal.archives-ouvertes.fr/hal-02397054`.

[2] Scanavino, M., "Design and testing methodologies for UAVs under extreme environmental conditions," Ph.D. thesis, Politecnico di Torino, 2021.

[3] Kunz, P. J., "Aerodynamics and design for ultra-low Reynolds number flight," Ph.D. thesis, Standford University, 2003.

[4] Ali, M., "Development and validation of a reduced order method for the study of flow on a rotor," Master's thesis, Politecnico di Torino, 2021.

[5] Van Garrel, A., "Development of a wind turbine aerodynamics simulation module," 2003.

[6] Marten, D., Lennie, M., Pechlivanoglou, G., Nayeri, C. N., and Paschereit, C. O., "Implementation, optimization, and validation of a nonlinear lifting line-free vortex wake module within the wind turbine simulation code qblade," *Journal of Engineering for Gas Turbines and Power*, Vol. 138, No. 7, 2016.

[7] Carreño Ruiz, M., Scanavino, M., D'Ambrosio, D., Guglieri, G., and Vilardi, A., "Experimental and numerical analysis of multicopter rotor aerodynamics," *AIAA Aviation 2021 Forum*, 2021.

[8] Russell, C. R., and Sekula, M. K., "Comprehensive analysis modeling of small-scale uas rotors," *AHS International 73rd Annual Forum, Fort Worth, TX*, 2017.

[9] Langtry, R. B., and Menter, F. R., "Correlation-based transition modeling for unstructured parallelized computational fluid dynamics codes," *AIAA journal*, Vol. 47, No. 12, 2009, pp. 2894–2906.

[10] Menter, F. R., "Two-equation eddy-viscosity turbulence models for engineering applications," *AIAA Journal*, Vol. 32, No. 8, 1994, pp. 1598–1605. https://doi.org/10.2514/3.12149, URL https://doi.org/10.2514/3.12149.

[11] Selig, M., "Low Reynolds number airfoil design lecture notes," *VKI Lecture Series, November*, 2003, pp. 24–28.

[12] Manavella, A., "Low Reynolds number propeller performance validation by CFD analysis and reduced order models," Master's thesis, Politecnico di Torino, 2021.

[13] Drela, M., "XFOIL: An analysis and design system for low Reynolds number airfoils," *Low Reynolds number aerodynamics*, Springer, 1989, pp. 1–12.

[14] M.C., G., and M.R., V., "Implicit Large Eddy Simulation of Low-Reynolds-Number Transitional Flow Past the SD7003 Airfoil," *40th Fluid Dynamics Conference and Exhibit*, edited by AIAA, Chicago, Illinois, 2010.

[15] A., U., P.-O., P., M., D., and J., P., "Implicit Large Eddy Simulation of Transitional Flows Over Airfoils and Wings," *19th AIAA Computational Fluid Dynamics*, 2009. AIAA 2009-4131.

[16] Desert, T., Moschetta, J.-M., and Bézard, H., "Numerical and experimental investigation of an airfoil design for a Martian micro rotorcraft," *International Journal of Micro Air Vehicles*, Vol. 10, No. 3, 2018, pp. 262–272.

[17] McCormick, B. W., *Aerodynamics of V/STOL flight*, Courier Corporation, 1999.

[18] Carreño Ruiz, M., and D'Ambrosio, D., "Aerodynamic Optimization of Quadrotor Blades Operating in the Martian Atmosphere," *AIAA 2022 SCITECH*, 2022(Accepted).

[19] Bézard, H., Désert, T., Jardin, T., and Moschetta, J.-M., "Numerical And Experimental Aerodynamic Investigation Of A Micro-UAV For Flying On Mars," *76th Annual Forum & Technology Display*, 2020.

[20] Hariharan, N. S., Egolf, T. A., and Sankar, L. N., "Simulation of rotor in hover: Current state, challenges and standardized evaluation," *52nd Aerospace Sciences Meeting*, 2014, p. 0041.

[21] Bhagwat, M. J., and Leishman, J. G., "Generalized viscous vortex model for application to free-vortex wake and aeroacoustic calculations," *Annual forum proceedings-American helicopter society*, Vol. 58, American Helicopter Society, Inc, 2002, pp. 2042–2057.

[22] Sant, T., "Improving BEM-based Aerodynamic Models in Wind Turbine Design Codes," Ph.D. thesis, Delft University of Technology, 2007.

[23] Argus, F. J., Ament, G. A., and Koning, W. J., "The Influence of Laminar-Turbulent Transition on Rotor Performance at Low Reynolds Numbers," *VFS Technical Meeting on Aeromechanics for Advanced Vertical Flight*, 2020.